Controlling the thermal conductance of graphene/*h*-BN lateral interface with strain and structure engineering

Zhun-Yong Ong,* Gang Zhang, and Yong-Wei Zhang
*Institute of High Performance Computing, A*STAR, Singapore 138632, Singapore*
(Received 21 July 2015; revised manuscript received 13 November 2015; published 2 February 2016)

Although phonon-mediated thermal conduction in pristine graphene and hexagonal boron nitride is well understood, less is known about phonon transport in single-sheet graphene-hexagonal boron nitride (Gr/*h*-BN) lateral heterostructures, where the thermal resistance of the interfaces plays an important role in the overall thermal conductivity. We apply the newly developed extended atomistic Green's function method to analyze with detail the effect of strain and structure engineering on the thermal conductance G_{int} of the Gr/*h*-BN interface. Our calculations show that longitudinal tensile strain leads to significant G_{int} enhancement (up to 25% at 300 K) primarily through the improved alignment of the flexural acoustic phonon bands, despite the reduction in the longitudinal acoustic (LA) and transverse acoustic phonon velocities. In addition, we find that alternating C-N zigzag bonds along the zigzag interface lead to a greater G_{int} than C-B bonds through more effective transmission of high-frequency LA and transverse optical phonons, especially at high strain levels. We also demonstrate how the interfacial structure dramatically affects the orientation of the transmitted optical phonons, a phenomenon that is neither seen for acoustic phonons nor predictable from conventional acoustic wave scattering theory. Insights from our paper can provide the basis for manipulating the interfacial thermal conductance in other two-dimensional heterostructures.

DOI: 10.1103/PhysRevB.93.075406

I. INTRODUCTION

One of the recent major advances in the integration of atomically thin films into nanoelectronics has been the spatially controlled synthesis of graphene-hexagonal boron nitride (Gr/*h*-BN) lateral heterostructures in which electrically conducting graphene (Gr) and insulating hexagonal boron nitride (*h*-BN) are combined to form a mechanically continuous sheet with lateral heterojunctions between them [1,2]. This result represents an important step towards the development of integrated circuitry based on atomically thin two-dimensional (2D) materials. In such atomically thin circuits, it is envisioned that interconnects between the active devices are formed from regular strips of very highly conductive monolayer graphene separated by continuous domains of *h*-BN. In spite of its one-atom thickness, the high electrical conductivity of graphene [3] allows it to support a sufficiently large current so that multiple devices can be embedded within a single sheet. In addition, because of the weak interlayer van der Waals forces [4], vertical stacking of these single-sheet circuits offers a possible path to building more complex three-dimensionally integrated nanoscale circuits.

However, in spite of the advantages of having electrically conductive and insulating elements embedded in a continuous one-atom thick sheet, the confined volume of such nanoscale structures can lead to high current densities and concentrated Joule heating potentially detrimental to device performance, necessitating a more careful look at the thermal conductive properties of such heterostructures given the importance of dissipating locally generated hot spots [5]. The problem of heat dissipation is fortunately partly offset by the high thermal conductivity of graphene, which has been shown to be an excellent material for spreading heat [6]. On the other hand, the weak van der Waals interlayer interaction typical of 2D materials means that the thermal conductance between the sheet and the substrate is low, around $20\,\text{MWK}^{-1}\,\text{m}^{-2}$ for the graphene-SiO_2 interface [7,8]. Thus, given the low thermal conductivity [5] of amorphous SiO_2 ($\sim 1\,\text{WK}^{-1}\,\text{m}^{-1}$), the thermal healing length, which is the characteristic length scale of the temperature decay in the film as a result of heat transfer to the substrate and is associated with the size of a device that predominantly dissipates heat via the substrate, is roughly of the order of 0.1 μm for graphene [5]. Furthermore, the thermal healing length is unlikely to change significantly even if other channels of thermal dissipation, such as the coupling between electrons and substrate optical phonons [9], are included. For devices of dimensions smaller than the thermal healing length, resistance to lateral heat dissipation poses a greater challenge than direct heat sinking to the substrate. Therefore, since the waste heat can only be effectively channeled *within* each sheet in such small devices, the boundary between graphene and *h*-BN poses a potentially significant source of interfacial thermal (Kapitza) resistance that can impede phonon-mediated heat diffusion.

It is expected that within each single-sheet circuit, there could be multiple Gr/*h*-BN interfaces given that the individual logic devices would be linked with graphene interconnects. The structure of the interface can also differ according to the orientation of the graphene interconnects, which depends on the circuit layout. For example, an interconnect supporting charge transport in the zigzag direction would have interfaces along its armchair edges and vice versa. In addition, because of the difference in the lattice constants of graphene and *h*-BN, the synthesis of such in-plane junctions with full lattice registration [10] can introduce strains that affect the Kapitza resistance. Previous molecular dynamics (MD) simulations of thermal transport in Gr/*h*-BN superlattices [11–13] suggest

*Corresponding author: ongzy@ihpc.a-star.edu.sg

that the Gr/h-BN interfacial orientation exerts a significant effect on the scattering and transmission of phonons although the exact transmission mechanism at each interface remains imprecisely understood because of the limitations of the MD technique. Therefore, controlling phonon-mediated heat diffusion in such Gr/h-BN single-sheet heterostructures requires an in-depth appreciation of the Kapitza resistance phenomenon, in addition to knowing the thermal conductivities of pure graphene [14–16] and BN [17,18]. Understanding the role of strain in interfacial thermal conductance can also provide fresh physical insights to inspire new strategies for controlling the thermal conductance of interfaces. Although there is considerable amount of work done to understand the effect of strain on the thermal conductivity of graphene [19,20], the effects of strain on Kapitza conductance remains poorly understood.

In order to understand the dependence of the Kapitza conductance on the interface and strain, it is necessary to establish first the basic theoretical framework underpinning our subsequent discussion of phonon-mediated interfacial heat transfer. At the fundamental level, heat transfer and phonon transmission at the interface between two solid insulators are primarily mediated by a two-phonon elastic process in which a phonon on one side with a specific wave vector and polarization is scattered across the boundary with a finite probability to another phonon state on the other side with a different wave vector and polarization at the same frequency. This scattering process thus depends on the phonon dispersion, which determines the available out-going and in-coming phonon channels, and the structure of the interface that governs the probability of transition between the phonon states. It naturally follows that the Kapitza resistance should vary with the application of tensile strain since the latter modifies the phonon dispersion by changing the interatomic bond length and interaction strength.

In this paper, we work within this framework to explore the dependence of the Gr/h-BN interfacial thermal (Kapitza) conductance on these properties using our recently developed extension [21] of the well-known Atomistic Green's Function (AGF) method, which was used previously to study coherent phonon transport in nanostructures [22–24] but has been reformulated so that the transmission probability of individual phonon modes can be efficiently computed. This new method yields the exact reciprocal space (k_x, k_y) composition of the transmitted acoustic and optical phonons, enabling us to sharpen our theoretical analysis of the fundamental interfacial heat transfer physics. For instance, we are able to quantify the transmission probability of the optical phonon modes, which was previously not accessible with other methods such as the acoustic mismatch model (AMM), and to show that they contribute substantially to the Kapitza conductance. Therefore, we are able to relate precisely the variation in the composition of transmitted phonons, induced by tensile strain or differences in the interfacial structure, to the change in the Kapitza conductance.

II. METHODOLOGY

In our paper, we study two types of *smooth* Gr/h-BN interfaces: the armchair and the zigzag interface. The Gr/h-BN armchair interface, which has both C-N and C-B bonds between the armchair edges of graphene and BN, is shown in Fig. 1(a). The zigzag interface, on the other hand, consists of two zigzag edges joined together with four possible interfacial configurations, which are shown in Figs. 1(b)–1(e). While being relevant to the actual Gr/h-BN boundary, these smooth interfaces also represent an ideal model system for studying the physics underlying interfacial thermal conductance and allow us to introduce the relevant physical concepts that we expect

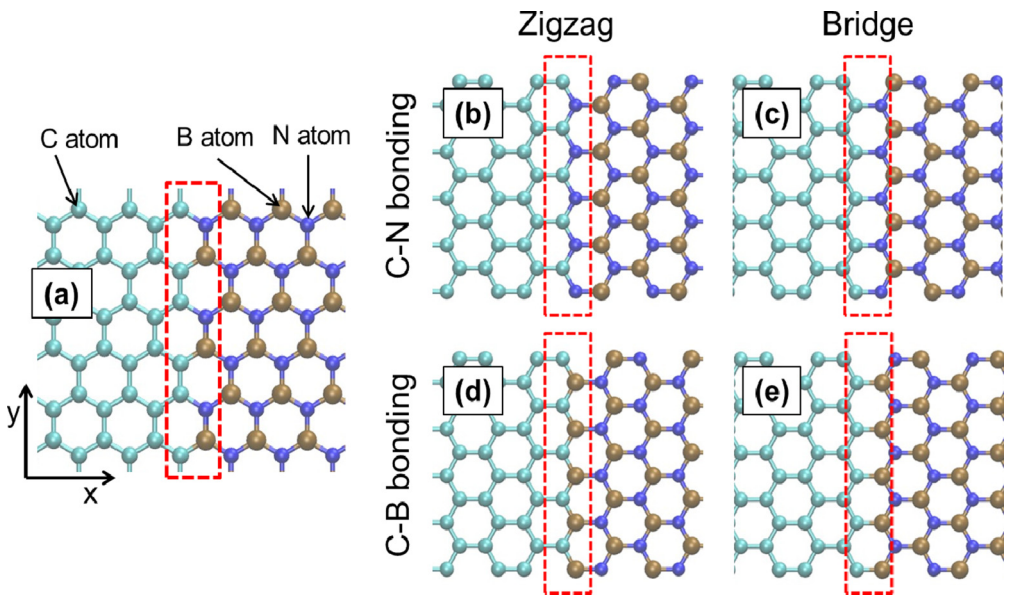

FIG. 1. Schematic of the Gr/h-BN (a) armchair interface and the zigzag interface for (b) C-N zigzag, (c) C-N bridge, (d) C-B zigzag, and (e) C-B bridge bonding at the interface.

to be adapted for analyzing the same phenomenon in other interfacial systems (e.g., between [25] 1T-MoS_2 and 2H-MoS_2).

We adopt in the rest of the paper the convention where the x axis (y axis) is normal (parallel) to the interface so that the longitudinal (transverse) direction is parallel to the x axis (y axis). The direction of the heat conduction is along the x direction. We construct and prepare the Gr/h-BN structures in the same manner as in Ref. [21].

To model the interactions between atoms, we use the C-B-N parameters for the Tersoff potential [26] given in Ref. [11] where the thermal conductivity of the Gr/h-BN superlattice is estimated from MD simulations. The structure is optimized using the code GULP [27], which is also used to compute the force constant matrices in our transmission calculations. To find the most stable heterostructure configuration that is planar, we first determine the minimum lattice constant for pure graphene and pure h-BN separately by comparing the values of the total energy and the phonon frequencies at different bond lengths, as computed in GULP. We find that the C-C bond length in planar graphene has a minimum value of 1.439 Å as bonds shorter than this value would result in imaginary phonon frequencies. Likewise, the minimum B-N bond length in planar h-BN is 1.46 Å. Thus, to prevent any corrugation of the heterostructure especially on the BN side, we create the heterostructure in which the C-C and B-N bond lengths are all set at 1.46 Å. We take this heterostructure to be the 0%-strain configuration. However, because of the lattice mismatch between graphene and h-BN, there is some residual tensile stress. After the atomic coordinates are set, the heterostructure is optimized again in GULP.

The conductance of the entire lateral heterostructure can be calculated using the Landauer formula [24],

$$G = \frac{1}{2\pi S}\int_0^\infty d\omega\, \hbar\omega \frac{dN}{dT}\Xi(\omega), \tag{1}$$

where S, $\hbar$, N, and Ξ are the cross-sectional area, the Planck constant divided by 2π, the Bose-Einstein distribution function, and the phonon transmission function, respectively. The detailed procedure for calculating the transmission function $\Xi(\omega)$ is fairly involved and will not be described here. Instead we refer the reader to our previous paper [21], where it is given in more detail. Here, we give a brief description of the extended atomistic Green's function technique [21] used to compute the transmission coefficients. The heterostructure consists of a finite scattering region, the Gr/h-BN interface, coupled to semi-infinite leads, one of which is pure graphene (left) and the other pure h-BN (right). At each given frequency, the bulk phonon modes of each lead are obtained by extracting the Bloch matrix [21], which describes the translational symmetry in the bulk Green's function, from its surface Green's function. The phonon eigenmodes and their corresponding wave vectors are computed from the eigenvectors of the Bloch matrix. The available *extended* phonon eigenmodes give us the scattering channels in the graphene or h-BN where the phonon are scattering into or out of. We can describe the right-going phonon heat current as consisting of phonons originating from the channels in the graphene left lead being scattered quantum mechanically to the channels in the h-BN right lead with a finite transition probability. Likewise, the left-going phonon heat current consists of phonons being scattered from the channels in the h-BN right lead to the channels in the graphene left lead. Once we have the phonon eigenmodes, we can calculate the t matrix, the elements of which give us the transition probability distribution between the graphene channels in the left lead and the h-BN channels in the right lead. Hence, at each frequency, we can associate with each channel (or phonon eigenmode) a transmission coefficient between 0 and 1, which is equal to the sum of the transition probabilities associated with that eigenmode, and the transmission function $\Xi(\omega)$ used in Eq. (1), which is equal to the transmission function in the original AGF method [24], can be obtained by summing the transmission coefficients over the transverse wave vectors and different phonon branches.

Given that phonon transport is ballistic within the atomistic Green's function formalism, the Kapitza conductance $G_{\rm int}$ is estimated through the formula [21,23,28],

$$\frac{1}{G_{\rm int}} = \frac{1}{G_{\rm Gr/h\text{-}BN}} - \frac{1}{2G_{\rm Gr}} - \frac{1}{2G_{\rm BN}}, \tag{2}$$

where $G_{{\rm Gr}/h\text{-}{\rm BN}}$, $G_{\rm Gr}$, and $G_{\rm BN}$ are the conductance for the Gr/h-BN heterostructure, pristine graphene, and pristine BN, respectively. It follows that the thermal resistance of the interface or the left-hand side of the expression in Eq. (2) automatically reduces to zero when we replace BN with graphene or vice versa.

III. RESULTS

A. Strain dependence of Kapitza conductance of the armchair interface

We study the armchair interface first because it has only one interfacial bonding configuration, which simplifies the analysis of the strain effect on the Kapitza conductance. The temperature dependence of the thermal conductance $G_{\rm int}$ is shown in Fig. 2 for tensile strain in the (a) x and (b) y direction. Generally, $G_{\rm int}$ increases with temperature, reaching $3.52 \times 10^9\,{\rm WK^{-1}\,m^{-2}}$ at 300 K and 0% strain, which is roughly equivalent to the thermal resistance of 100 nm of BN [18] or 500 nm of graphene [15].

What is more striking is the *change* in the temperature dependence of $G_{\rm int}$ when tensile strain is applied, which we can interpret in terms of changes to the composition of the transmitted phonons. At low temperatures ($T \ll 100$ K), the strain dependence of $G_{\rm int}$ is insignificant. However, as we increase the temperature, the strain dependence and the *enhancement* in $G_{\rm int}$ become more pronounced especially for strain in the x direction. At room temperature (300 K), a 7% strain in the x direction yields a 27.4% increase in $G_{\rm int}$ while the same strain in the y direction corresponds to a significantly smaller 9.3% increase. However, at even higher temperatures, the relative increase in $G_{\rm int}$ with strain is much smaller and can even decrease in the case of the y directional strain in Fig. 2(b).

This strain-induced enhancement in the interfacial conductance is remarkable given that the application of strain is known to reduce the group velocities of the longitudinal acoustic (LA) and transverse acoustic (TA) phonon modes in graphene [19,29]. Naively, this group velocity reduction suggests that $G_{\rm int}$ should decrease with strain rather than increase as our results in Fig. 2(a) show, since the potential contribution to the interfacial heat flux by each LA and TA phonon mode

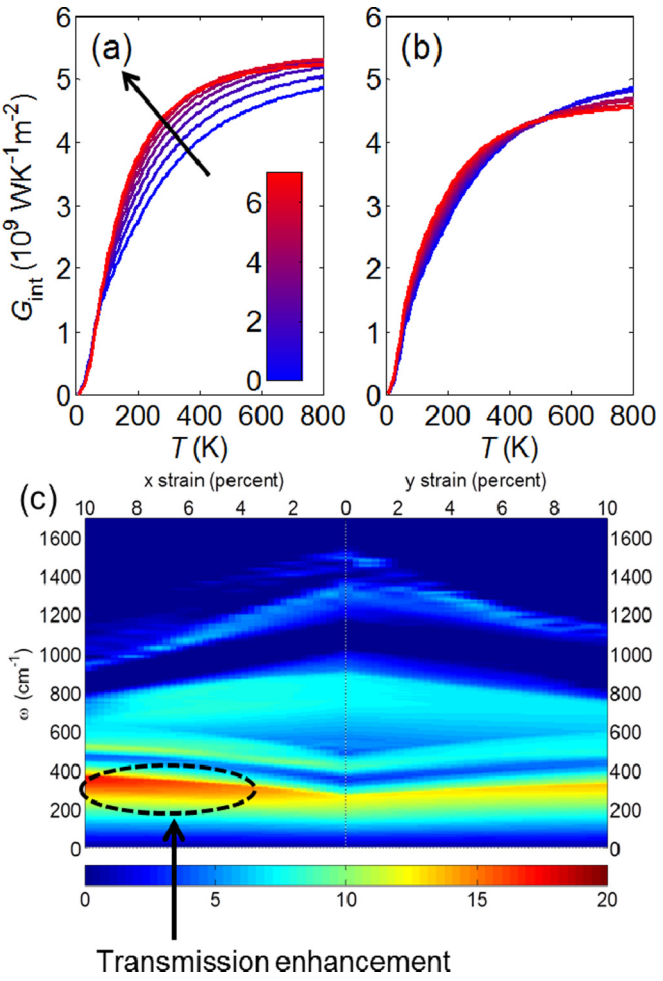

FIG. 2. The interfacial thermal conductance G_{int} as a function of temperature with increasing strain, from 0 to 7% in the (a) x and (b) y direction. The arrow indicates the direction of increasing strain. (c) The cross-sectional phonon transmission spectrum (nm^{-2}) for strain in the zigzag (x) and armchair (y) direction.

is expected to be reduced. To understand this counterintuitive strain-induced enhancement in G_{int} in terms of the composition of transmitted phonons, we plot the phonon transmission per unit cross-section area as a function of strain in the x and y direction in Fig. 2(c). The low-frequency ($\omega < 200\,\mathrm{cm}^{-1}$) portion of the transmission spectrum does indeed show a very slight reduction at higher strain because of the strain-induced reduction in the acoustic phonon group velocities. Thus, at low temperatures, heat conduction is mediated by phonons populating the much lower frequency range, which are little affected by the strain, and hence, G_{int} is only weakly dependent on strain.

On the other hand, we observe that x-directional strain leads to a pronounced transmission enhancement in the frequency range of $250-400\,\mathrm{cm}^{-1}$, although the corresponding transmission enhancement for y-directional strain is significantly weaker. Thus, as the temperature rises, the phonon population in the $250-400\,\mathrm{cm}^{-1}$ range grows, resulting in a higher G_{int}. Nevertheless, the overall transmission spectrum becomes narrower when the applied x- or y-directional tensile strain increases because of the strain-induced reduction in the transmission of the high-frequency optical phonons in addition to the decrease in the LA and TA phonon group velocities. Hence, at higher temperatures where the contribution from high-frequency phonons becomes more substantial, the total heat conductance decreases with strain, especially at strains higher than 5%, with the decrease in G_{int} induced by y-directional strain being more conspicuous [as can be seen in Fig. 2(b)] because of the weaker low-frequency transmission enhancement.

What is the origin of this phonon transmission enhancement in the $250-400\,\mathrm{cm}^{-1}$ frequency range suggested by the transmission spectrum in Fig. 2(c)? To answer this question, it is helpful to have a more detailed analysis of the composition of the transmitted phonons in terms of their wave vectors and polarization. We decompose the total phonon transmission in terms of the transmission probability of individual graphene and BN phonon modes distributed in (k_x, k_y, ω) space. Figure 3 shows the transmission probability distribution for phonons at normal incidence to the interface, corresponding to the $k_y = 0$ slice in (k_x, k_y, ω) space, at (a) 0 and (b) 5% x-directional strain. The left and right halves of the plot correspond to graphene and BN, respectively, and their LA, transverse acoustic (TA), and flexural acoustic (ZA) phonon branches are labeled to facilitate discussion on the role of the different phonon channels in thermal transport. An overall view of the distribution of the transmitted in-plane and out-of-plane graphene modes in (k_x, k_y, ω) space can be viewed in Figs. 3(e)–3(h).

Figures 3(c) and 3(d) show the constant frequency ($\omega = 200\,\mathrm{cm}^{-1}$) transmission spectrum in (k_x, k_y) space. As noted in Ref. [21], the loci of the ZA phonon modes in graphene and BN form a wider arc in (k_x, k_y) space than the loci of the LA and TA modes, indicating a greater proportion of states available for transmission. In addition, the low-frequency ZA phonon transmission probabilities are also close to unity because of the close overlap and alignment of their ZA phonon bands. Therefore, the acoustic phonon transmission in the low-frequency range is dominated by the ZA phonons in graphene and BN. We also note that the dispersion of the ZA phonon branch in Figs. 3(a) and 3(b) is linear rather than quadratic like in the ideal case. This is due to the strain caused by the lattice mismatch between graphene and h-BN in the heterostructure and has been reported in Refs. [20,29,30].

However, the frequency range of transmitted ZA phonons is limited by a cutoff that is determined by the ZA phonon band alignment between graphene and BN. In graphene at 0% strain [Fig. 3(a)], the cutoff is around $325\,\mathrm{cm}^{-1}$ while at 5% strain [Fig. 3(b)], it increases to around $392\,\mathrm{cm}^{-1}$. A comparison of Figs. 3(a) and 3(b) reveals that the higher cutoff is primarily due to the strain-induced blue-shift of the ZA phonons in BN, which increases the frequency overlap between the ZA phonon bands of graphene and BN. One also finds a similar increase in the transmission frequency cutoff for the TA phonons although their contributions to the interfacial conductance are much smaller. Therefore, we attribute the transmission enhancement in the $250-400\,\mathrm{cm}^{-1}$ frequency range and the longitudinal strain-induced increase in the room-temperature G_{int} to the better alignment of the ZA phonon bands between graphene and BN.

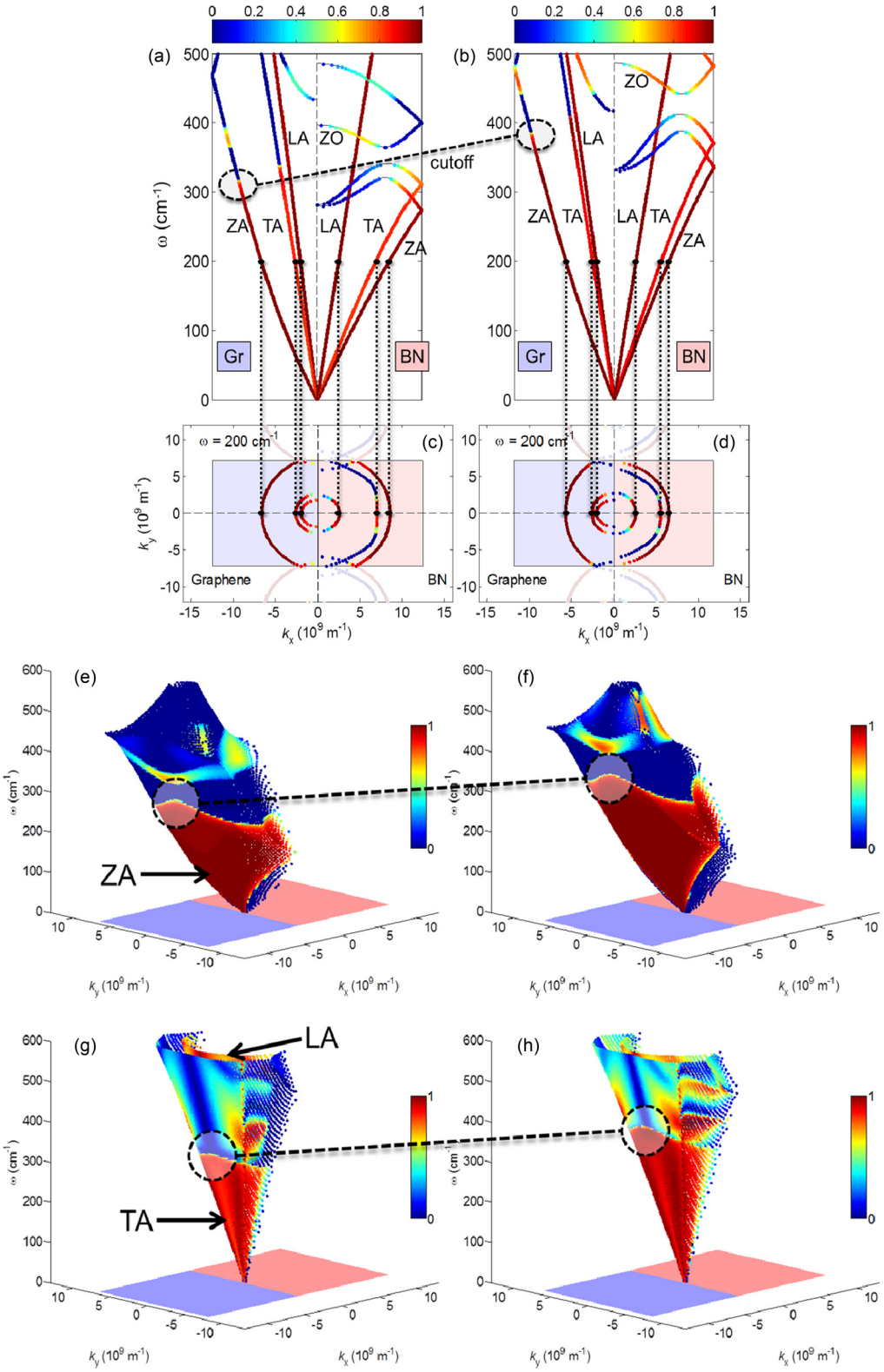

FIG. 3. Phonon dispersion in the longitudinal (zigzag) or x direction for graphene and BN, on the left and right half of the (k_x, ω) plane, respectively, at (a) 0% and (b) 5% longitudinal strain. The transmission probabilities of the modes are indicated in color. The corresponding distribution of modes on the (k_x, k_y) plane at $\omega = 200\,\mathrm{cm}^{-1}$ for (c) 0% and (d) 5% longitudinal strain are shown below. As a visual guide, we connect with the intersecting points between (a), (b) and (c), (d) with dotted lines. The transmission frequency cutoff for the ZA phonons is around 325 and 392 cm^{-1} for (a) and (b), respectively, and is indicated by the dashed lines. We also show the transmission probability spectra for the graphene out-of-plane phonon modes at (e) 0% and (f) 5% longitudinal strain in reciprocal and frequency space. (g) and (h) Corresponding transmission probability spectra for graphene in-plane (transverse and longitudinal acoustic) phonon modes at 0% and 5% strain, respectively. The dashed lines indicate the position of the transmission frequency cutoff.

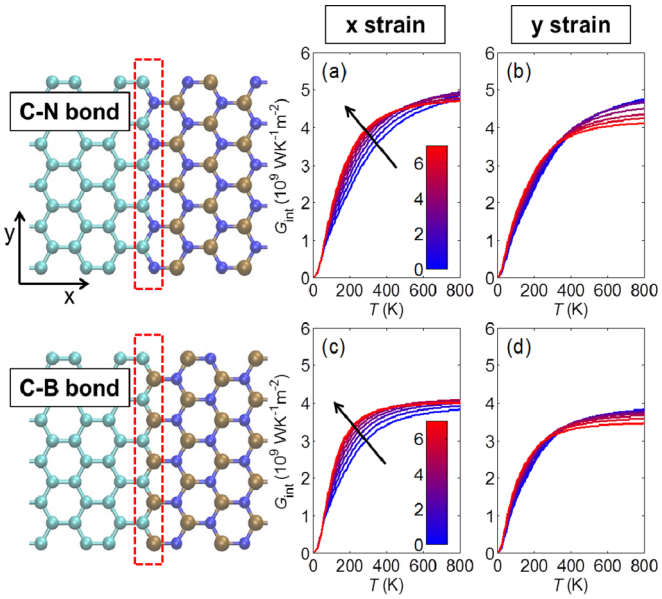

FIG. 4. Interfacial thermal conductance G_{int} as a function of temperature with increasing strain, from 0 to 7%, for the (a), (b) C-N and (c), (d) C-B zigzag interface, in the (a), (c) x direction and (b), (d) y direction. We have C-N or C-B zigzag bonds at the interface.

B. Strain dependence of Kapitza conductance of the zigzag interfaces

Having studied the Kapitza conductance of the armchair interface, we turn to the strain dependence of the Kapitza conductance of the smooth *zigzag* interface with different types of interfacial bonding. Figure 4 shows two configurations of the zigzag interface with identical orientations—one with alternating C-N bonds along the zigzag interface and the other with alternating C-B bonds. We call these interfacial bond configurations zigzag bonds. The two other possible configurations of the zigzag interface have parallel C-N and C-B bridge bonds [see Figs. 1(c) and 1(e)], but we do not study their strain dependence because our simulations show that the C-N and C-B bridge bonds rupture when the average applied strain exceeds 5%, although we study Kapitza conductance later in this letter. By comparing the results for the zigzag interface with C-N or C-B zigzag bonds, we can determine the effects of interfacial structure and bonding on interfacial heat transfer as well as how these effects change with strain.

Figure 4 shows the results for the G_{int} as a function of temperature at different values of x- and y-directional strain for C-N and C-B zigzag bonds. At 0% strain, the room temperature G_{int} is 3.42×10^9 WK^{-1} m^{-2} and 3.05×10^9 WK^{-1} m^{-2} for C-N and C-B zigzag bonds, respectively, which is slightly lower than the G_{int} for the armchair interface (3.52×10^9 WK^{-1} m^{-2}). Like the Gr/h-BN armchair interface, the increase in G_{int} is greater for x-directional strain than for y-directional strain. At 7% x-directional strain and 300 K, G_{int} increases by 23.6 and 21.0% for C-N and C-B bonding, respectively. Their transmission spectra at normal incidence for 0 and 5% strain are shown in Fig. 5. Our analysis shows that this G_{int} enhancement is due to the closer alignment of the ZA phonon bands at higher x-directional strain, similar to what we find for the armchair interface. Another similarity to

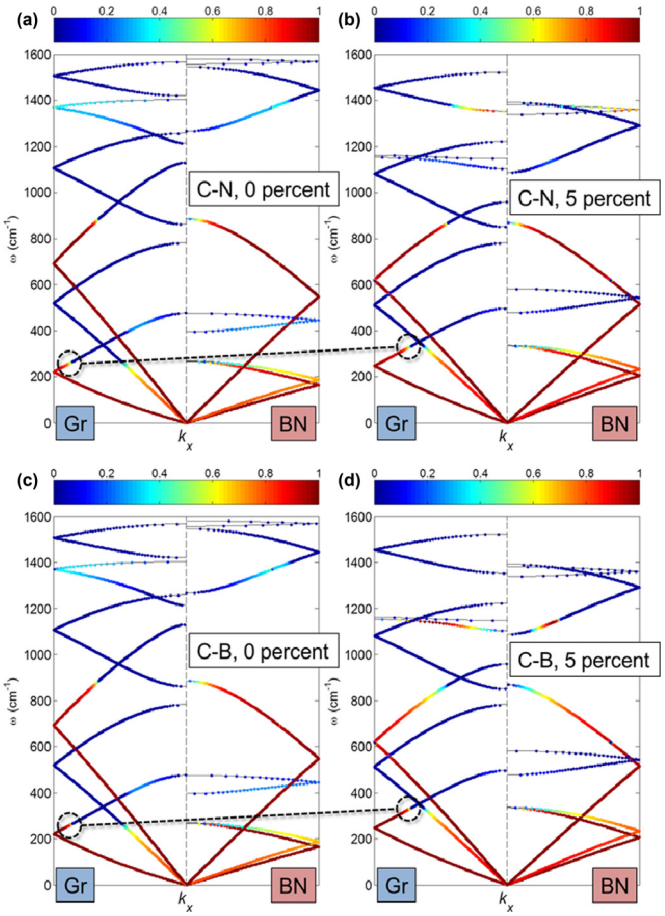

FIG. 5. Transmission probability spectra at normal incidence ($k_x = 0$) for BN and graphene at 0 and 5% longitudinal (x) strain, similar to that given in Figs. 3(a) and 3(b), corresponding to the (a), (b) C-N and (c), (d) C-B zigzag bonds, over the frequency range of $0-1600\,\mathrm{cm}^{-1}$.

the armchair interface is the weak dependence on strain at low temperatures.

Interestingly, at temperatures above 200 K, the G_{int} for C-N zigzag bonds and the G_{int} for C-B zigzag bonds begin to diverge, pointing to a difference in the composition of phonons being transmitted across the interface. Figures 6(a) and 6(b) show the variation in the total transmission spectrum with respect to the x-directional strain for C-N and C-B zigzag bonds. In the low-frequency range ($\omega < 600\,\mathrm{cm}^{-1}$), the transmission spectra for C-N and C-B zigzag bonds are almost identical. This allows us to rule out the possibility that the discrepancy in G_{int} is due to differences in ZA phonon transmission.

However, Figs. 6(a) and 6(b) show salient differences between the two spectra at higher frequencies. At 0% strain, transmission in the $1200 - 1350\,\mathrm{cm}^{-1}$ range is significantly higher for C-N bonding than for C-B bonding, although, as with the armchair interface, the phonon contribution in this frequency range rapidly diminishes as longitudinal strain increases. Another prominent difference is the transmission in the $800 - 1050\,\mathrm{cm}^{-1}$ range, which is significantly larger for C-N bonding. This suggests that the high-temperature G_{int} differences between Figs. 4(a) and 4(c) are due to the difference

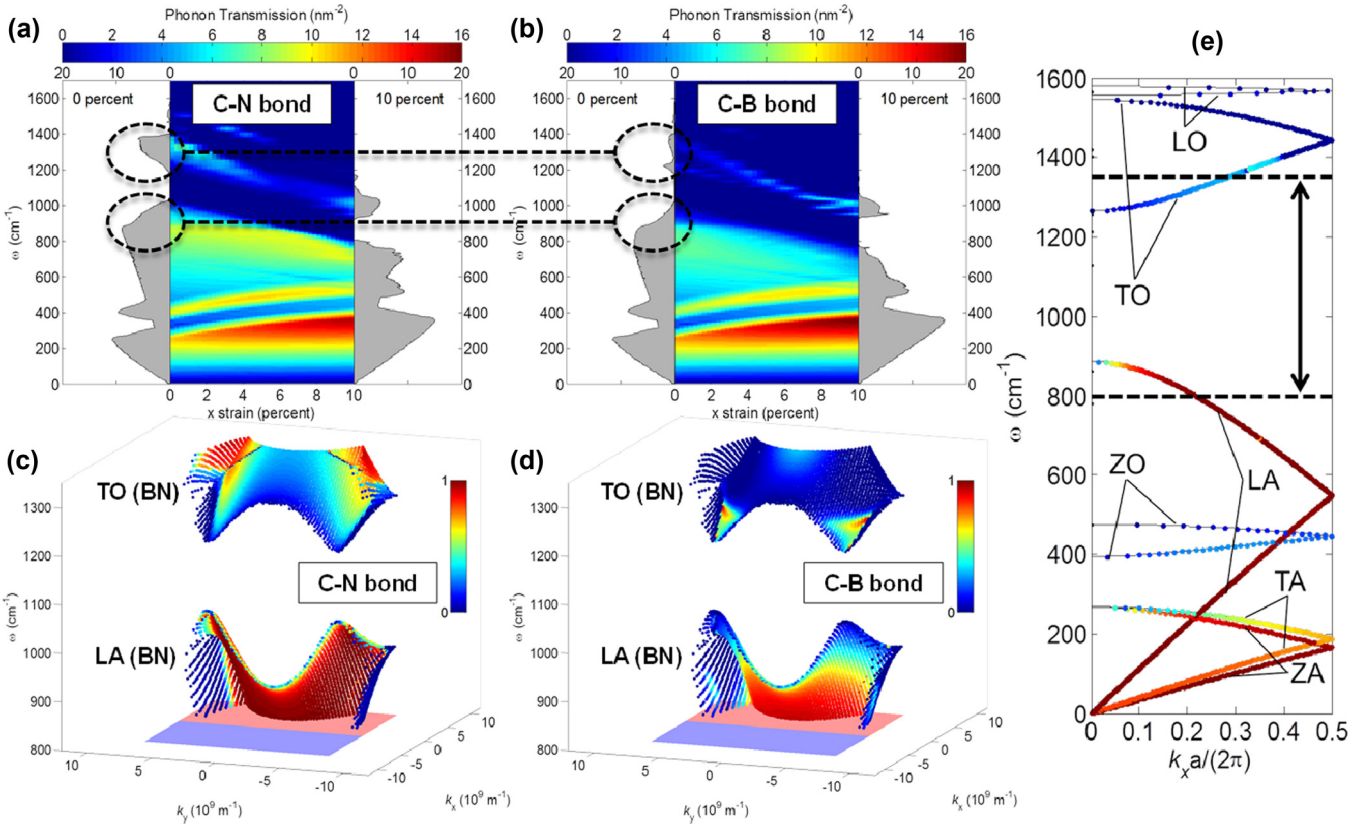

FIG. 6. Cross-sectional phonon transmission as a function of strain in the armchair direction (normal to the zigzag interface) for (a) the C-N and (b) the C-B interfacial bond. (c) and (d) Corresponding BN phonon transmission probability spectra at 0% strain in (ω, k_x, k_y) space and in the $800 - 1350\,\mathrm{cm}^{-1}$ range, which includes the LA and TO phonon bands. (e) The phonon dispersion in the direction normal to the interface showing the phonon transmission probabilities. The dashed lines show the lower and upper bound of the $800 - 1350\,\mathrm{cm}^{-1}$ frequency range. We also label the LA, TA, ZA, LO, TO, and ZO bands in BN. There are 12 phonon branches instead of six because we define the unit cell with four atoms in our AGF computational scheme. However, it is straightforward to identify the branches because they are connected at $k_x = 0$.

in phonon transmission over the $800 - 1350\,\mathrm{cm}^{-1}$ frequency range.

To identify the origin of this high-frequency transmission enhancement, we plot in Figs. 6(c) and 6(d) the BN phonon transmission probability spectrum in reciprocal space over the $800 - 1350\,\mathrm{cm}^{-1}$ frequency range at 0% strain for C-N and C-B bonding. In this frequency range, it is immediately clear that the phonon transmission on the BN side is dominated by modes in the higher frequency LA phonon and the TO phonon bands, which we identify from the phonon dispersion in Fig. 6(e). Another distinctive feature of the transmission spectra for the TO phonon band is that most of the strongly transmitted modes are not at normal incidence to the interface, i.e., they have a finite k_y component. The transmission probability distribution in these phonon bands is noticeably weaker for C-B bonding. Therefore, we attribute the difference in the G_{int} to the difference in the transmission of the modes at the top of the LA phonon band and in the TO phonon band. In other words, the change in the zigzag bond type exerts a much stronger influence on the transmission of high frequency phonons than on low frequency acoustic phonons.

In addition, the difference in the transmission of these LA and TO phonon modes becomes more pronounced at higher longitudinal strains. In BN, as the strain is increased, the bottom of the TO phonon band and the top of the LA phonon band shift downwards in frequency because of the strain-induced reduction in the LA phonon group velocities. This is clearly seen in Fig. 7, which shows the same spectra as in Figs. 6(c) and 6(d) but with the frequencies downshifted at 5 and 10% longitudinal strain. We observe two transmission phenomena associated with this strain increase. The first is the reduction in the transmission probability of the higher frequency LA phonons. This reduction is especially pronounced for the zigzag interface with C-B bonds and may be due to the weaker strength of the C-B bond relative to the C-N bond [11]. The second is the phonon transmission enhancement at the bottom of the TO band and is more unusual. More interesting, if we compare Figs. 7(c) and 7(d), we find that the enhancement is greater for TO phonon modes away from normal incidence for C-N zigzag bonds but is concentrated in modes closer to normal incidence for C-B zigzag bonds. This suggests that the angular distribution of the transmitted optical phonons is much more sensitive to the structure of the interface than that for acoustic phonons. In addition, there is a preferential orientation in the transmitted optical phonons that can be associated with the interfacial structure, unlike the case for the transmitted acoustic phonons

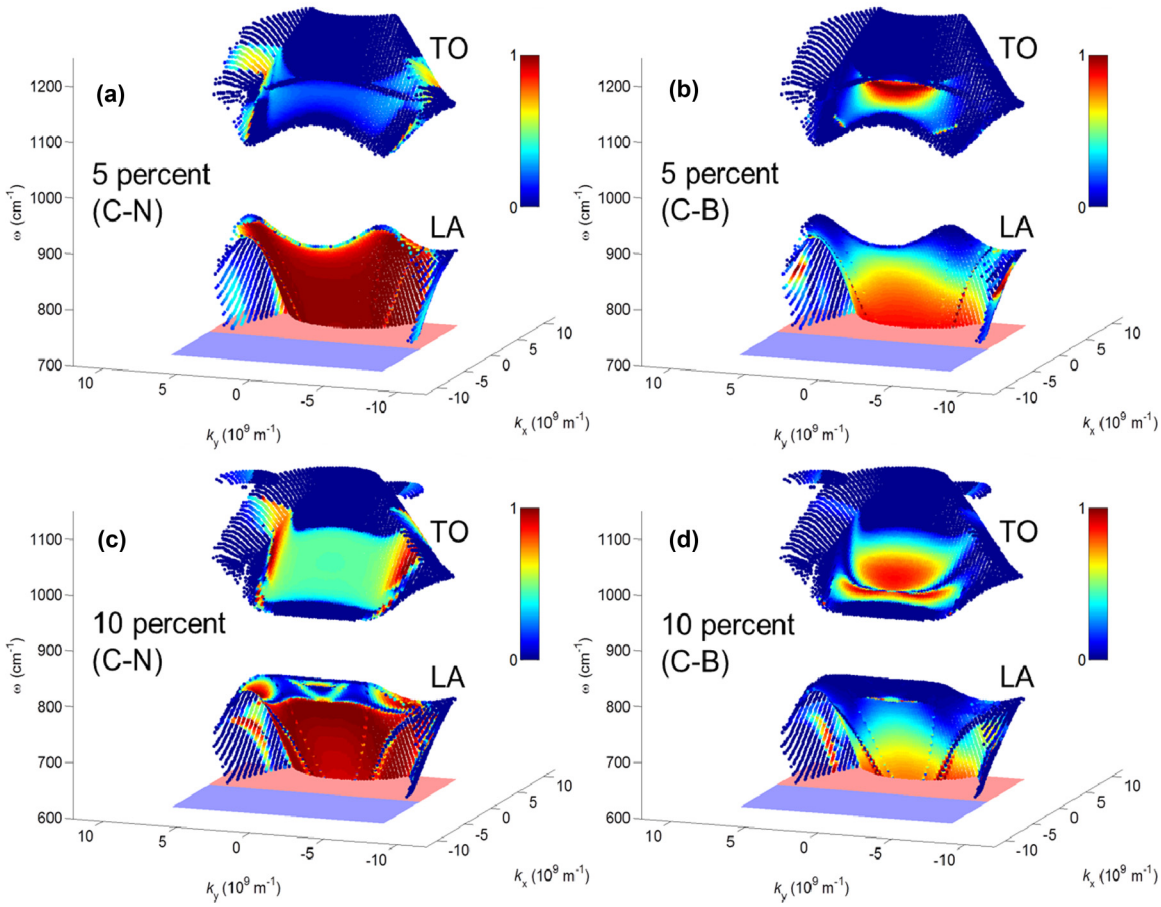

FIG. 7. (a) and (b) Corresponding BN phonon transmission probability spectra at 5% strain in (k_x, k_y, ω space and in the $700 - 1250\,\mathrm{cm}^{-1}$ range, which includes the LA and TO phonon bands. (c) and (d) The same BN phonon transmission probability spectra but at 10% strain.

where the wavelength, polarization, and group velocity of the incident phonons play a much more important role.

C. Interfacial bond orientation dependence

Given that the sensitivity of the orientation of the transmitted higher frequency LA and TO phonons to the bonding type at the zigzag interface, we probe more into the effects of the interfacial structure on phonon transmission. Let us recall that there are two possible interfacial bond orientations for the smooth Gr/h-BN zigzag interface. The first consists of alternating C-N or C-B bonds (zigzag bonds for short), which we studied in the previous section, while the second consists of parallel bridgelike C-N or C-B bonds (bridge bonds for short). To compare the effect of the interfacial structure (bond type and orientation) on the thermal conductance, we plot their G_{int} as a function of temperature at 0% strain in Fig. 8(a). We find that the interface with bridge bonds exhibits a higher conductance at lower temperatures than the interface with zigzag bonds, although the difference diminishes as the temperature increases. The G_{int} for the zigzag-bond orientation also shows a large difference in terms of the bond type with the C-N bond type yielding a significantly higher conductance. However, for the interface with the bridge-bond orientation, the conductance does not vary significantly with the bond type, and the interface with C-B bridge bonds in fact exhibits a slightly higher conductance. To determine the physical origin

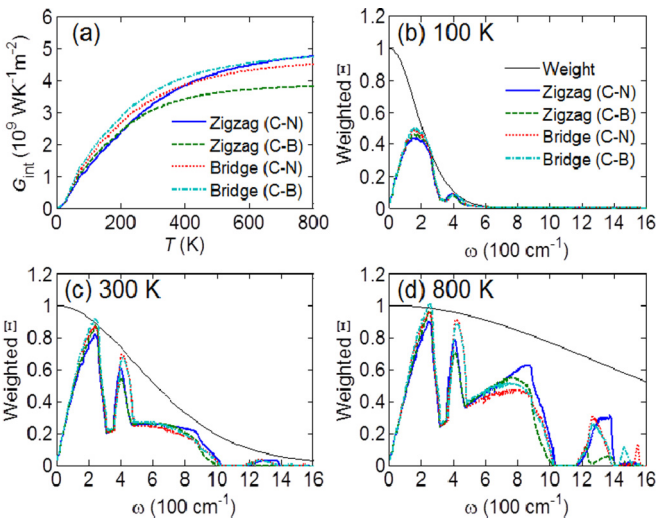

FIG. 8. (a) Interfacial thermal conductance G_{int} as a function of temperature from 0–800 K for C-N/C-B zigzag and bridge bonds. We calculate the temperature-weighted phonon transmission at (b) 100, (c) 300, and (d) 800 K.

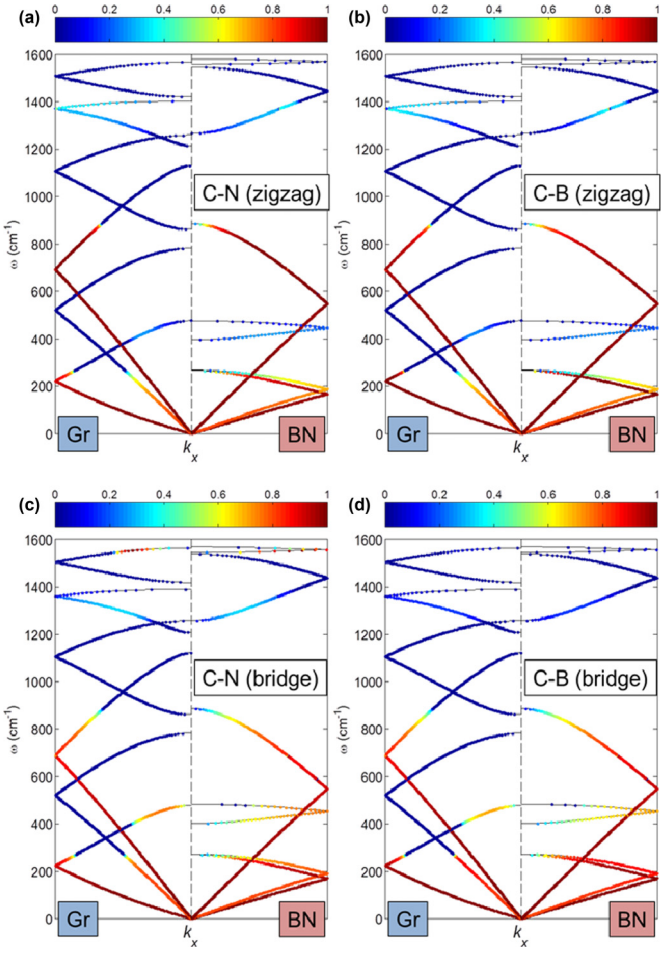

FIG. 9. Transmission probability spectra at normal incidence ($k_x = 0$) for BN and graphene at 0 percent strain, corresponding to the (a) C-N and (b) C-B zigzag bonds as well as to the (c) C-N and (d) C-B bridge bonds, over the frequency range of 0–1600 cm^{-1}.

of the difference in conductance, we plot in Figs. 8(b)–8(d) the temperature-weighted transmission spectra, which we define as $\hat{\Xi}(T,\omega) = \frac{\hbar\omega}{k_B}\frac{dN}{dT}\Xi(\omega)$, which yields the expression $\lim_{T\to\infty}\hat{\Xi}(T,\omega) = \Xi(\omega)$ in the high temperature limit. A comparison of the transmission spectra at normal incidence in Fig. 9 with the $T = 300\,\mathrm{K}$ spectra in Fig. 8(b) shows that the interface with C-N or C-B bridge bonds is slightly more efficient at transmitting the ZA and TA phonons between BN and graphene at low temperature. There is also greater elastic phonon scattering between the graphene ZA phonon band and the BN flexural optical (ZO) phonon band. However, the contribution from the $\omega > 600\,\mathrm{cm}^{-1}$ range of the transmission spectrum for C-N zigzag bonding [Figs. 8(c) and 8(d)] starts to dominate at higher temperatures. Thus, at higher temperatures, the difference between the G_{int} for C-N zigzag bonds and C-N/C-B bridge bonds diminishes. This result highlights the importance of the optical phonon contribution to the Kapitza conductance.

IV. SUMMARY AND CONCLUSION

We summarize our key findings of our theoretical study of thermal conduction at the Gr/h-BN interface as follows:

(1) In spite of the reduction in the group velocities of the LA and TA phonons, the application of strain in the direction of the heat flow enhances the conductance primarily through improved alignment of the ZA phonon bands in graphene and BN. The transmission of the acoustic phonons is strongly dependent on their polarization, frequency, and wave vector direction.

(2) The transmission of high-frequency optical phonons can be strongly reduced by strain because of the misalignment of their optical phonon bands.

(3) Variations in the bond orientation and type at the interface primarily affect the scattering and transmission of higher frequency modes. In the case of the transmission of the transverse optical (TO) phonons for the zigzag-bond interface (see Fig. 7), the bonding type can dramatically affect the preferred orientation of the transmitted optical phonons: the strained C-N bond enhances transmission preferentially away from the normal incidence while the strained C-B bond concentrates transmission along the normal incidence.

From the above findings, we are able to abstract two rather general physical principles in interfacial heat transfer. The first is that the application of strain modifies the alignment of the phonon bands in the materials that comprise the interface and changes what phonon channels are available for the two-phonon elastic scattering process. The second is that the structure of the interface controls the probability of scattering between these available phonon channels. These factors should also be considered in the analysis of the Kapitza conductance between other materials. It should be mentioned that our paper is limited to two-phonon scattering processes and that nonlinear phenomena such as rectification [31–33] are beyond the scope and capabilities of the computational techniques used in this paper.

ACKNOWLEDGMENT

We acknowledge the financial support provided by the Agency for Science, Technology and Research (Singapore).

[1] M. P. Levendorf, C.-J. Kim, L. Brown, P. Y. Huang, R. W. Havener, D. A. Muller, and J. Park, Graphene and boron nitride lateral heterostructures for atomically thin circuitry, Nature **488**, 627 (2012).

[2] Z. Liu, L. Ma, G. Shi, W. Zhou, Y. Gong, S. Lei, X. Yang, J. Zhang, J. Yu, K. P. Hackenberg, A. Babakhani, J.-C. Idrobo, R. Vajtai, J. Lou, and P. M. Ajayan, In-plane heterostructures of graphene and hexagonal boron nitride with controlled domain sizes, Nat Nano **8**, 119 (2013).

[3] M. V. Fischetti, J. Kim, S. Narayanan, Z.-Y. Ong, C. Sachs, D. K. Ferry, and S. J. Aboud, Pseudopotential-based studies of electron transport in graphene and graphene nanoribbons, J. Phys.: Condens. Matter **25**, 473202 (2013).

[4] Y. Shi, W. Zhou, A.-Y. Lu, W. Fang, Y.-H. Lee, A. L. Hsu, S. M. Kim, K. K. Kim, H. Y. Yang, L.-J. Li, J.-C. Idrobo, and

J. Kong, van der Waals epitaxy of MoS_2 layers using graphene as growth templates, Nano Lett. **12**, 2784 (2012).

[5] E. Pop, Energy dissipation and transport in nanoscale devices, Nano Research **3**, 147 (2010).

[6] A. A. Balandin, Thermal properties of graphene and nanostructured carbon materials, Nat Mater **10**, 569 (2011).

[7] K. F. Mak, C. H. Lui, and T. F. Heinz, Measurement of the thermal conductance of the graphene/SiO_2 interface, Appl. Phys. Lett. **97**, 221904 (2010).

[8] M.-H. Bae, Z.-Y. Ong, D. Estrada, and E. Pop, Imaging, simulation, and electrostatic control of power dissipation in graphene devices, Nano Lett. **10**, 4787 (2010).

[9] Z.-Y. Ong, M. V. Fischetti, A. Y. Serov, and E. Pop, Signatures of dynamic screening in interfacial thermal transport of graphene, Phys. Rev. B **87**, 195404 (2013).

[10] P. Sutter, R. Cortes, J. Lahiri, and E. Sutter, Interface formation in monolayer graphene-boron nitride heterostructures, Nano Lett. **12**, 4869 (2012).

[11] A. Kınacı, J. B. Haskins, C. Sevik, and T. Çağın, Thermal conductivity of BN-C nanostructures, Phys. Rev. B **86**, 115410 (2012).

[12] T. Zhu and E. Ertekin, Phonon transport on two-dimensional graphene/boron nitride superlattices, Phys. Rev. B **90**, 195209 (2014).

[13] J. Song and N. V. Medhekar, Thermal transport in lattice-constrained 2D hybrid graphene heterostructures, J. Phys.: Condens. Matter **25**, 445007 (2013).

[14] A. A. Balandin, S. Ghosh, W. Bao, I. Calizo, D. Teweldebrhan, F. Miao, and C. N. Lau, Superior thermal conductivity of single-layer graphene, Nano Lett. **8**, 902 (2008).

[15] L. Lindsay, D. A. Broido and N. Mingo, Flexural phonons and thermal transport in graphene, Phys. Rev. B **82**, 115427 (2010).

[16] J. H. Seol, I. Jo, A. L. Moore, L. Lindsay, Z. H. Aitken, M. T. Pettes, X. Li, Z. Yao, R. Huang, D. Broido, N. Mingo, R. S. Ruoff, and L. Shi, Two-dimensional phonon transport in supported graphene, Science **328**, 213 (2010).

[17] I. Jo, M. T. Pettes, J. Kim, K. Watanabe, T. Taniguchi, Z. Yao, and L. Shi, Thermal conductivity and phonon transport in suspended few-layer hexagonal boron nitride, Nano Lett. **13**, 550 (2013).

[18] L. Lindsay and D. A. Broido, Enhanced thermal conductivity and isotope effect in single-layer hexagonal boron nitride, Phys. Rev. B **84**, 155421 (2011).

[19] L. Lindsay, W. Li, J. Carrete, N. Mingo, D. A. Broido, and T. L. Reinecke, Phonon thermal transport in strained and unstrained graphene from first principles, Phys. Rev. B **89**, 155426 (2014).

[20] L. F. C. Pereira and D. Donadio, Divergence of the thermal conductivity in uniaxially strained graphene, Phys. Rev. B **87**, 125424 (2013).

[21] Z.-Y. Ong and G. Zhang, Efficient approach for modeling phonon transmission probability in nanoscale interfacial thermal transport, Phys. Rev. B **91**, 174302 (2015).

[22] Z. Huang, J. Y. Murthy, and T. S. Fisher, Modeling of polarization-specific phonon transmission through interfaces, J. Heat Transfer **133**, 114502 (2011).

[23] A. Y. Serov, Z.-Y. Ong, and E. Pop, Effect of grain boundaries on thermal transport in graphene, Appl. Phys. Lett. **102**, 033104 (2013).

[24] W. Zhang, T. S. Fisher, and N. Mingo, The atomistic Green's function method: an efficient simulation approach for nanoscale phonon transport, Numerical Heat Transfer, Part B: Fundamentals **51**, 333 (2007).

[25] R. Kappera, D. Voiry, S. E. Yalcin, B. Branch, G. Gupta, A. D. Mohite, and M. Chhowalla, Phase-engineered low-resistance contacts for ultrathin MoS_2 transistors, Nat Mater **13**, 1128 (2014).

[26] J. Tersoff, New Empirical Model for the Structural Properties of Silicon, Phys. Rev. Lett. **56**, 632 (1986).

[27] J. D. Gale and A. L. Rohl, The General Utility Lattice Program (GULP), Mol. Simul. **29**, 291 (2003).

[28] Z. Tian, K. Esfarjani, and G. Chen, Enhancing phonon transmission across a Si/Ge interface by atomic roughness: First-principles study with the Green's function method, Phys. Rev. B **86**, 235304 (2012).

[29] N. Bonini, J. Garg, and N. Marzari, Acoustic phonon lifetimes and thermal transport in free-standing and strained graphene, Nano Lett. **12**, 2673 (2012).

[30] T. Zhu and E. Ertekin, Resolving anomalous strain effects on two-dimensional phonon flows: The cases of graphene, boron nitride, and planar superlattices, Phys. Rev. B **91**, 205429 (2015).

[31] A. A. Maznev, A. G. Every, and O. B. Wright, Reciprocity in reflection and transmission: What is a 'phonon diode'?, Wave Motion **50**, 776 (2013).

[32] D. Segal, Single Mode Heat Rectifier: Controlling Energy Flow Between Electronic Conductors, Phys. Rev. Lett. **100**, 105901 (2008).

[33] L.-A. Wu and D. Segal, Sufficient Conditions for Thermal Rectification in Hybrid Quantum Structures, Phys. Rev. Lett. **102**, 095503 (2009).